Low energy (e,2e) studies from CH_4: Results from symmetric coplanar experiments and molecular three-body distorted wave theory

K. L. Nixon,[1,a)] Andrew J. Murray,[1] Hari Chaluvadi,[2] Chuangang Ning,[3] and D. H. Madison[2]

[1]*Photon Science Institute, School of Physics and Astronomy, University of Manchester, Oxford Road, Manchester M13 9PL, United Kingdom*

[2]*Department of Physics, Missouri University of Science and Technology, Rolla, Missouri 65409, USA*

[3]*Department of Physics and Key Laboratory of Atomic and Molecular NanoSciences of MOE, Tsinghua University, Beijing 100084, People's Republic of China*

(Received 1 March 2011; accepted 2 April 2011; published online 2 May 2011)

Low energy experimental and theoretical triply differential cross sections are presented for electron impact ionization of methane (CH_4) for both the highest occupied molecular orbital (HOMO) and next highest occupied molecular orbital (NHOMO). The HOMO is a predominantly p-type orbital which is labeled $1t_2$ and the NHOMO is predominantly s-type labeled $2a_1$. Coplanar symmetric (symmetric both in final state electron energies and observation angles) are presented for final state electron energies ranging from 2.5 to 20 eV. The theoretical M3DW (molecular three-body distorted wave) results are in surprisingly good agreement with experiment for the HOMO state and less satisfactory agreement for the NHOMO state. The molecular NHOMO results are also compared with the ionization of the 2s shell of neon which is the isoelectronic atom. © *2011 American Institute of Physics*. [doi:10.1063/1.3581812]

I. INTRODUCTION

Electron scattering from molecules is a rich field with many important applications [Ref. 1 and references therein]. As an example, electron–molecule collisions are widely used in the technology industry for plasma devices and etching; they have an important role in developing more accurate medical imaging techniques and radiotherapies and natural phenomena such as auroras, planetary nebula, and lightning also critically dependent on electron–molecule collisions. Understanding each of these processes requires accurate and detailed information of the collision dynamics between the electron and the target molecule. (e,2e) experiments which measure electron impact ionization, provide the most rigorous experimental data in the form of a triple differential cross section (TDCS). At low impact energies the probability of ionization is highest. As such, collisions in this energy region occur most abundantly and so it is important to characterize the interactions fully to describe the physical phenomena that are seen. Despite this, detailed experimental and theoretical examinations of electron–molecule collisions in this regime have been relatively few. This is due to the challenges presented to both theory and experiment when working in this energy regime and is also due to the nature of molecules, which are used as the targets. At low energies the collision dynamics are far from impulsive and so effects such as post collision interactions, multiple collisions, target polarization, and distortion of the associated wavefunctions of the target and electrons involved in the interaction all must be considered and evaluated. These challenges have been largely overcome for atomic targets and sophisticated theoretical models have been developed which provide good agreement with experimental data for many atoms.[2–4]

Adopting molecules as the target in these studies is significantly more complicated. Generating experimental and theoretical data that can be directly compared is considerably more involved. One problem that arises is that molecules tend to have more closely spaced energy levels compared to atoms and these states are often unresolvable by experiment.[5–8] In this case, the measured TDCS arises from multiple orbitals making comparison with theory less conclusive. A further consideration that arises in most experiments is that the target molecules are randomly oriented in space, due to being produced from either an effusive gas beam or oven. This random orientation needs to be included in the theory before a direct comparison with experimental data can be attempted. Finally, molecules have multiple distributed nuclei that may each act as independent scattering centres. This noncentral distribution considerably complicates the model due to a reduction of symmetry and makes the calculations computationally intensive. Notwithstanding these challenges, theoretical models are being developed for application to polyatomic molecules in the low energy regime and new experimental measurements are emerging [see Refs. 5–14 for examples of recent work]. A review of recent experimental and theoretical work for electron-impact ionization of molecules was given by Madison and Al Hagan.[15]

Methane (CH_4) is the smallest hydrocarbon and so is a relatively simple polyatomic molecule. It has a highly symmetric tetrahedral structure with four equivalent C–H bonds. There are five molecular orbitals in the X^1A_1 ground state. Molecular symmetry leads to triple degeneracy of the $1t_2$ highest occupied molecular orbital (HOMO), the lower orbitals being the $2a_1$ and $1a_1$ orbitals. This simple electronic

a)Electronic mail: Kate.Nixon-2@manchester.ac.uk.

structure has made methane an ideal prototype to model organic systems and so it has often been employed when developing models of biological matter or planetary atmospheres. Furthermore, methane is a potent greenhouse gas with a high global warming potential. This simple molecule also has significant technological uses such as in the development of plasma devices and in the fabrication of carbon nanotubes, nanowires, and graphene [see Refs.16–19 for examples]. In terms of the investigation instigated here, methane is an ideal target to help in understanding the discrepancies observed between experimental and theoretical data for molecules. The $2a_1$ next highest occupied molecular orbital (NHOMO) of methane has a very similar electron density to that of a carbon 2s atomic orbital.[20] As such, it is expected that this molecular orbital can be described by a much simpler atomic theory. More importantly, the $2a_1$ molecular orbital has s-electron characteristics and so has predominantly spherical symmetry. Any effects of the spherical averaging procedure utilized in a theoretical model should hence be minimized for such an orbital. A comparison between the experimental and theoretical data for this orbital should therefore reveal if the observed differences are due to this spherical averaging process. A further investigation of this premise, as carried out here, is to compare results from methane to the isoelectronic atom, neon. The atomic target clearly does not require spherical averaging within the theoretical model. Furthermore, this comparison should isolate key features seen in the TDCS due to the molecular nature of the target.

A number of (e,2e) studies of methane have been previously undertaken, mostly utilizing the high energy electron momentum spectroscopy (EMS) regime.[21–24] These studies demonstrate that accurate theoretical molecular wavefunctions are readily achievable. New studies of the collision dynamics from methane at intermediate energies were also carried out recently.[10,14]

The remainder of this paper is structured as follows: Sec. II outlines the pertinent feature of the (e,2e) spectrometer used to measure the triple differential cross sections, whereas Sec. III describes the theoretical model used to predict the cross section. The results for both experiment and theory are presented and compared in Sec. IV. Conclusions from this study are summarized in Sec. V.

II. EXPERIMENTAL APPARATUS

The coincidence data taken throughout this experimental study utilized the fully computer controlled and optimized (e,2e) spectrometer at the University of Manchester. This spectrometer has been described in detail elsewhere[25–27] and so only the features pertinent to this study are reproduced here. The spectrometer was operated in a "standard" coplanar geometry where the momenta of the ingoing and outgoing electrons are within the same plane. Figure 1 depicts the coplanar scattering geometry used. The two outgoing electron momentum analyzers were independently rotated around the detection plane to map the probability of a collision event. This probability map is termed the triple differential cross section. In this study, a symmetric configuration was used, so that $\xi_1 = \xi_2 = \xi$ and $E_1 = E_2 = E$.

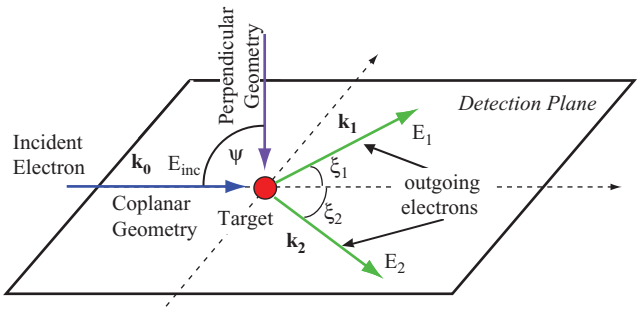

FIG. 1. Schematic of the scattering geometry depicting the various angles employed. A coplanar geometry ($\psi = 0°$) is defined when the momenta of all three electrons lie in the detection plane. The analyzer angles (ξ_1 and ξ_2) are measured with respect to the incident electron beam $\mathbf{k_0}$ in this plane. Noncoplanar geometries can also be accessed in this apparatus by lifting the electron gun out of the detection plane, although this feature was not utilized here.

High purity methane was admitted into the interaction region, controlled by a needle valve. Typical operating pressures of 9×10^{-6} Torr were used in the chamber, in conjunction with very low incident electron beam currents of ~70 nA, in order to achieve good signal to background ratios.

Computer control and optimization of the electrostatic lenses within the electron analyzers allowed the automated tuning of the spectrometer at each new analyzer angle throughout data collection. The energy of the spectrometer was calibrated at the start of each new measurement so as to ensure data were taken at the peak of the coincidence binding energy spectrum. This study focused on the two outermost molecular orbitals within methane: the highest occupied $1t_2$ orbital with a binding energy ~14 eV and the next highest occupied $2a_1$ orbital at ~23 eV binding energy. A typical coincidence binding energy spectrum for these two orbitals is shown in Fig. 2. The data in Fig. 2 were taken under the same conditions, however, in two separate measurements since the power supply used to vary, the incident electron energy could only scan 10 V. Figure 2 clearly demonstrates that the orbitals are fully resolved so that the coincidence data from each orbital is uncontaminated by its neighbor. These well resolved

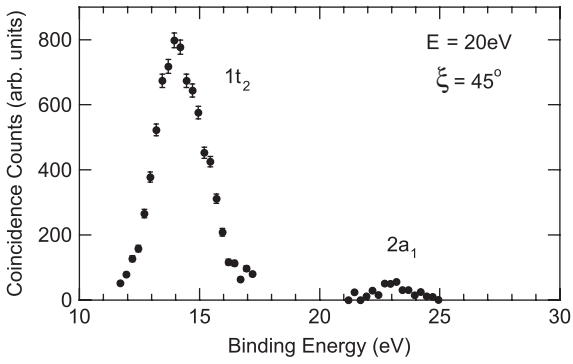

FIG. 2. A typical coincidence binding energy spectrum obtained for CH_4. These data were measured in a coplanar geometry with outgoing electron energies of 20 eV at $\xi = 45°$. The two peaks correspond to the two highest orbitals, i.e., the $1t_2$ and $2a_1$ orbitals as labeled. The orbitals are easily resolved, so that the TDCS from each orbital is uncontaminated by its neighbor. The width of the HOMO is significantly increased from that due solely to the experimental resolution due to Jan–Teller distortion.[21]

structures eliminate one of the difficulties often encountered when studying molecules, since the data from each orbital can be measured separately for comparison with theory. It is also seen that the coincidence signal from the $2a_1$ orbital is significantly smaller than from the $1t_2$ orbital.

The experimental data presented here have not been measured on an absolute scale. Hence, each data set has been normalized to unity at the peak. Each data set is derived from several sweeps of the electron analyzers around the detection plane, which were then averaged. The vertical error bars represent the standard error on this average, whereas the horizontal error bars represent the angular uncertainty due to the acceptance angle of the electron analyzers and the pencil angle of the electron gun.

III. THEORETICAL FRAMEWORK

The details of the molecular three-body distorted wave (M3DW) approximation have been presented elsewhere [28–30] so only a brief overview will be presented here. The M3DW TDCS is given by

$$\frac{d^5\sigma}{d\Omega_a d\Omega_b dE_b} = \frac{1}{(2\pi)^5}\frac{k_a k_b}{k_i}(|T_{\rm dir}|^2 + |T_{\rm exc}|^2 + |T_{\rm dir} - T_{\rm exc}|^2), \tag{1}$$

where $\vec{k}_i$ is the initial state wave vector, $\vec{k}_a$ ($\vec{k}_b$) is the wave vector for the scattered (ejected) electron, and the direct and exchange amplitudes are $T_{\rm dir}$ and $T_{\rm exc}$,respectively:

$$T_{\rm dir} = \langle \chi_a^-(\vec{k}_a, \mathbf{r}_1)\chi_b^-(\vec{k}_b, \mathbf{r}_2)C_{\rm scat-eject}(r_{12}) \times |V - U_i|\phi_{\rm DY}^{\rm OAMO}(\mathbf{r}_2)\chi_i^+(\vec{k}_i, \mathbf{r}_1)\rangle, \tag{2}$$

$$T_{\rm exc} = \langle \chi_a^-(\vec{k}_a, \mathbf{r}_2)\chi_b^-(\vec{k}_b, \mathbf{r}_1)C_{\rm scat-eject}(r_{12}) \times |V - U_i|\phi_{\rm DY}^{\rm OAMO}(\mathbf{r}_2)\chi_i^+(\vec{k}_i, \mathbf{r}_1)\rangle. \tag{3}$$

In Eqs. (2) and (3), $\mathbf{r}_1$ ($\mathbf{r}_2$) is the coordinate of the incident (bound) electron, χ_i, χ_a, and χ_b are the distorted waves for the incident, scattered, and ejected electrons, respectively, $C_{\rm scat-eject}$ is the Coulomb interaction between the scattered projectile and ejected electron, and $\phi_{\rm DY}^{\rm OAMO}$ is the Dyson orbital averaged over all orientations (OAMO—orientation averaged molecular orbital)[28] for the initial bound state wavefunction of the active electron. The molecular wavefunction was calculated using density functional theory along with the standard hybrid B3LYP[31] functional by means of the ADF 2007 (Amsterdam Density Functional) program[32] with the TZ2P (triple-zeta with two polarization functions) Slater type basis sets. For low energy electron-impact ionization, we have found that the full Coulomb interaction $C_{\rm scat-eject}$ typically over estimates the strength of the electron–electron repulsion while the Ward–Macek approximation[33] yields better agreement with experiment so we have used the Ward–Macek approximation in this work.

The potential V in Eqs. (2) and (3) is the initial state interaction between the projectile and the neutral molecule, and U_i is the initial-state spherically symmetric distorting potential which is used to calculate the initial-state distorted wave χ_i. The Schrödinger equation for the incoming electron wavefunction is given by

$$\left(T + U_i - \frac{k_i^2}{2}\right)\chi_i^+(\vec{k}_i, \mathbf{r}) = 0, \tag{4}$$

where T is the kinetic energy operator, and the "+'' superscript on $\chi_i^+(\vec{k}_i, r)$ indicates outgoing wave boundary conditions. The initial state distorting potential contains three components $U_i = U_S + U_E + U_{CP}$, where U_S is the initial state spherically symmetric static potential which is calculated from the molecular charge density averaged over all angular orientations, U_E is the exchange-distortion potential of Furness and McCarthy,[34] and U_{CP} is the correlation-polarization potential of Perdew and Zunger[35] (see also Padial and Norcross[36]).

The two final channel distorted waves are obtained from a Schrödinger equation similar to Eq. (4)

$$\left(T + U_f - \frac{k_{a(b)}^2}{2}\right)\chi_{a(b)}^-(\vec{k}_{a(b)}, \mathbf{r}) = 0. \tag{5}$$

Here $U_f = U_I + U_E + U_{CP}$ where U_I is the final state spherically symmetric static distorting potential for the molecular ion which is calculated using the same procedure as U_S except that the active electron is removed from the charge distribution.

For the $1t_2$ state, the Dyson orbital averaged over all orientations $\phi_{\rm DY}^{\rm OAMO}$ is zero due to the symmetry of the state (i.e., there are exactly canceling positive and negative contributions). To avoid this cancelation, we averaged the absolute value of the Dyson orbital instead of the actual orbital.

IV. RESULTS AND DISCUSSION

A. Accuracy of the OAMO wavefunctions

A reliable, accurate OAMO wavefunction for use as the $\phi_{\rm DY}^{\rm OAMO}$ can be obtained by noting that the high energy (e,2e) EMS experiment provides a measurement of the Dyson orbital.[37] EMS results represent the square modulus of the momentum space wavefunction, which is the Fourier transform of a radial wavefunction averaged over all orientations. Consequently, one way to generate an accurate wavefunction would be to take the inverse Fourier transform of experimental EMS data. However, since the measurement is directly related to the square of the wavefunction, a unique solution for the inverse problem cannot be obtained due to cross terms. Alternatively, the accuracy of the OAMO wavefunctions used in the M3DW theory can be evaluated by taking its Fourier transform and then comparing it with EMS data. Figure 3 compares the square modulus of the Fourier transform of the $\phi_{\rm DY}^{\rm OAMO}$ for the $1t_2$ and $2a_1$ states with the momentum wavefunctions measured by Clark *et al.*[21] It may be seen that there is reasonably good agreement with experiment for both states, which would indicate that the two averaging methods yield reasonable results. It is interesting and surprising to note that $1t_2$ state is in better agreement with the EMS measurements than the $2a_1$ state.

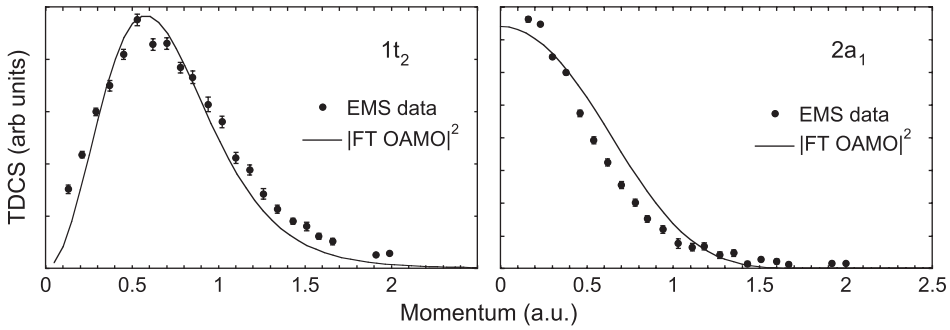

FIG. 3. Comparison between experimental EMS data (dots)[21] and the square modulus of the Fourier transform of the orientational averaged molecular wavefunctions, ϕ_{DY}^{OAMO}, (lines) which were used to calculate the TDCS used in this study.

B. Triple differential cross sections for methane

1. $1t_2$ state

The experimental and calculated TDCS for the outermost, $1t_2$, orbital of methane are shown in Fig. 4. There is reasonably good qualitative agreement between experiment and theory. Both sets of data show the typical trends seen for atomic targets, despite the molecular nature of methane. At the highest energy, with outgoing electron energies of 20 eV as shown in Fig. 4(a), a larger cross section is seen in the forward scattering direction ($\xi < 90^\circ$), compared to scattering in the backward direction ($\xi > 90^\circ$). This inverts as the energies are lowered, both in the theory and experiment. At the lowest energy of 2.5 eV [Fig. 4(f)], the largest relative amplitude is predicted in the backward direction; however, the apparatus cannot reach the scattering angles where this peaks. The theoretical prediction for the large angle peak position differs from that obtained experimentally.

As the energy of the outgoing electrons is lowered, it is expected that the Coulomb repulsion between outgoing electrons will play an increasingly important role, driving the electrons apart. This repulsion is called a post-collision-interaction (PCI). PCI would cause the forward scattering peak to shift toward $\xi = 90^\circ$ in symmetric kinematics as the outgoing electron energy lowers and the data presented here demonstrates this effect. PCI will also shift the backward scattering peak toward $\xi = 90^\circ$, however this cannot be confirmed in this data since the backwards peak is beyond the angular range accessible to the experiment in all cases.

Overall, agreement between the experimental data and theoretical calculations is reasonable given the complexity of the interactions at these energies and given the approximations that have been made as described in Sec. III. The peak positions for the forward scattering peak are in general well represented in the model. The movement of the forward peak toward $\xi = 90^\circ$, as the energy is lowered, is also reproduced. However, the backward scattering peak is predicted to be at lower scattering angles than is observed for all energies. Theory also predicts a deep minimum between the forward and backward peaks, whereas the data do not exhibit this. Further, the relative heights of the peaks for each incident energy are not in good agreement with the data. The relatively good agreement is, overall, surprising given the p-like symmetry of the $1t_2$ orbital, which has parity inversion through the

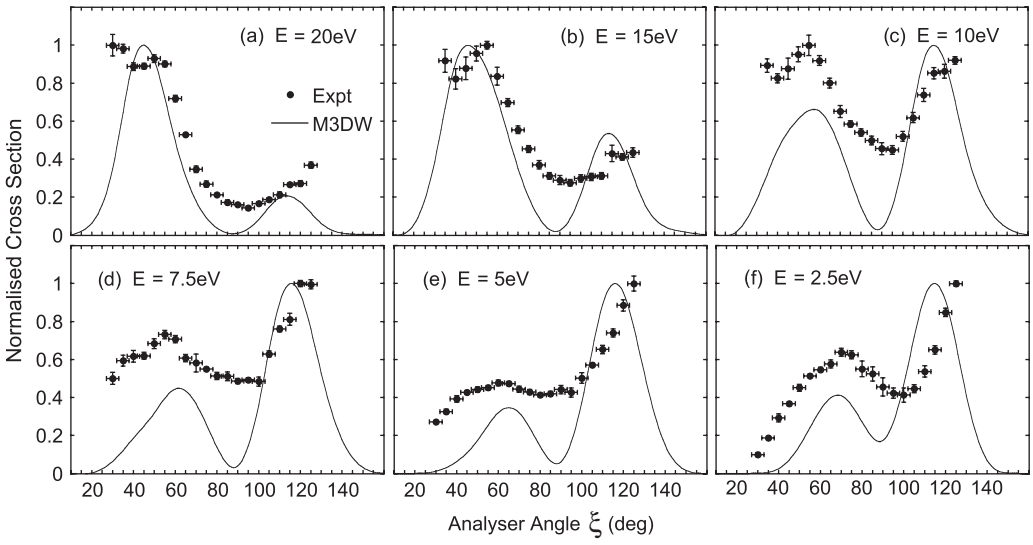

FIG. 4. TDCS from the $1t_2$ HOMO state of CH_4 for coplanar symmetric kinematics. The energies of the outgoing electrons are shown on the respective plots. The experimental data (dots) and results from the molecular three-body distorted wave approximation (lines) are depicted. The experimental and theoretical data have been independently normalised to unity at the peak for each energy.

molecular centre. This inversion symmetry has been lost in the averaging process so this approximation might be expected to cause significant differences between theory and experiment. It seems that the angular details of the bound state wavefunction must not be very important for low energies, although they may be the cause of some of the discrepancies that are seen.

2. $2a_1$ state

One of the key motivations for carrying out this study is that the $2a_1$ state of CH_4 is highly symmetric and has no parity inversion through the molecular centre. As such, it is expected that the approximations used in the spherical averaging process should be far less severe than for the $1t_2$ state. Figure 5 shows the results for the $2a_1$ state. Again, the data show behavior similar to atomic targets, with a forward and backward peak being observed. However, a major difference in the data for this state is in the evolution of the peak at angles $\sim \xi = 90^\circ$, a feature that is not usually seen in atomic targets. This feature is small at higher outgoing energies, but becomes increasingly clear and more pronounced as the energy is decreased. Peaks in this region (where the outgoing electrons emerge back to back, i.e., at $\xi = 90^\circ$), are often attributed to PCI between the two outgoing electrons; however, at the energies used here it is unlikely that PCI is the dominant cause. Further, the peak at $\xi = 90^\circ$ becomes more pronounced as the energy is lowered, rather than being due to a merger between the forward and backward peaks. This new feature must therefore be considered as being due to an additional scattering phenomena that arises for this state.

By contrast, the M3DW only predicts atomic-like structures, with a TDCS that differs little compared to that predicted for the $1t_2$ state. The model again produces two peaks, with a deep minimum between forward and backward scattering peaks. Although there is qualitative agreement between theory and experiment for the highest energies, theory does not predict the correct peak positions, relative heights or structure for the lower energies. In the spherical averaging process for the nuclei, the point charges from the hydrogen nuclei are spread out to a uniform distribution on a sphere which would make them much less effective as a scattering centre.[14] Consequently, the fact that the theory predicts two lobes while experiment has three lobes, suggests that the three lobe structure might originate from scattering from the H nuclei, but experimental data from neon presented in Sec. IV C indicate that other processes may also be playing a role in producing the peak at $\xi = 90^\circ$.

The limited agreement between experiment and theory for this state is surprising, given that this orbital was specifically selected for its almost spherical structure and lack of parity inversion. A contributing factor to this, given the relatively good agreement between theory and experiment for the $1t_2$ state, may be that the $2a_1$ state is deeper within the molecule (i.e., it is not the outermost orbital), so that scattering from the H nuclei may become more important, whereas the nuclei are more effectively screened for the outer $1t_2$ state.

Figure 6 shows the $1t_2$ and $2a_1$ theoretical results normalized to unity at the largest cross section. It is interesting to note that the results for the two states are very similar in structure (although they are different in their predicted magnitude, which is not seen in the comparison with the experimental data here due to normalization). This observation suggests that the main contributing factor to the calculated cross section for low energies is either the dynamics of the collision or the role of nuclear scattering which is the same for both molecular states and that the nature of the orbital does not have a significant influence on the theoretical predictions.

C. TDCS for isoelectronic atom and molecule

By comparing the TDCS for the $2a_1$ state in CH_4 (IP = 23.05 eV) with the isoelectronic atom neon (IP = 48.5 eV), it may be possible to identify sources of the discrepancy between experiment and theory shown above. Given that the $2a_1$ MO in methane is considered to be equivalent to

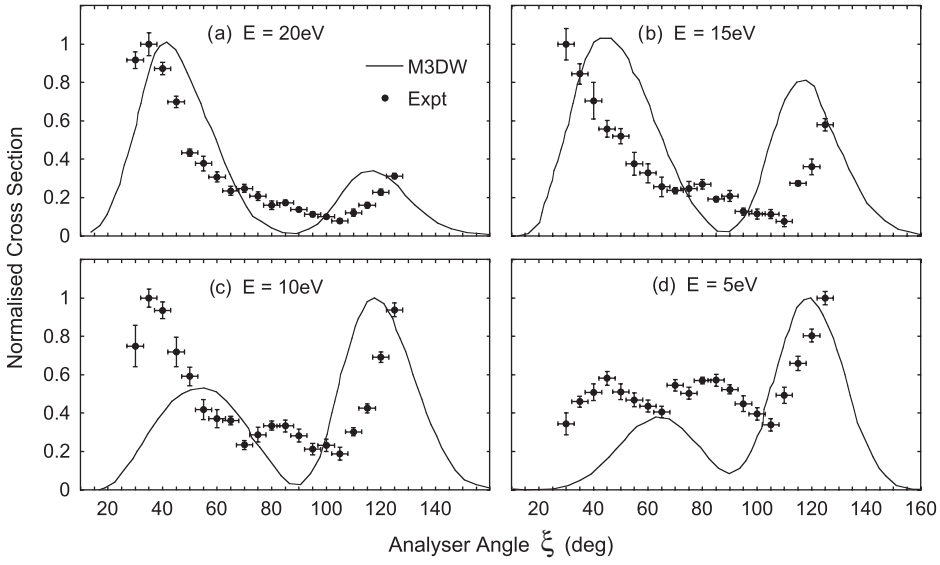

FIG. 5. As for Fig. 4, for the $2a_1$ NHOMO state of CH_4.

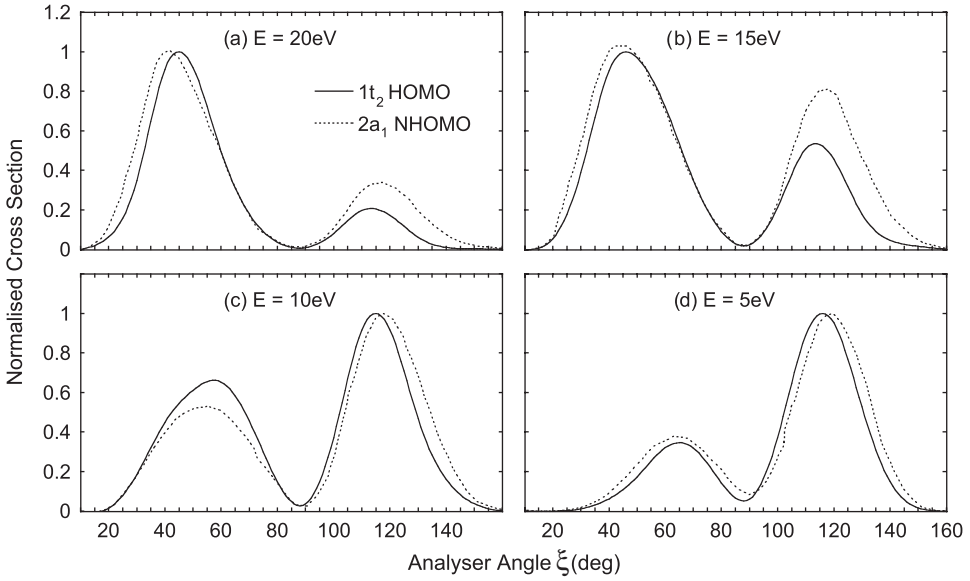

FIG. 6. A comparison of the TDCS from the M3DW calculation for the $1t_2$ (solid line) and $2a_1$ (dashed line) normalized to unity at the peak. The theory predicts very similar structure for both states, although the absolute magnitudes are different.

a relatively unaltered 2s carbon atomic orbital,[20] it is anticipated that the TDCS from the $2a_1$ state may be similar to that of the analogous 2s atomic state in neon, since in each case there are six electrons outside the 2s shell. A comparison of the TDCS of the molecule with that of neon could then indicate if the lack of agreement between experiment and theory is primarily due to the molecular nature of the target. Since the theoretical model does not need to apply spherical averaging for atoms, the effect of this approximation is eliminated. Further, differences in the data for the atom and molecule may also arise from the additional scattering centres of the hydrogen nuclei present in CH_4.

Figure 7 shows the TDCS for ionizing the $2a_1$ state of CH_4 and the Ne 2s state at two energies; one at a relatively high energy where the outgoing electrons both have an energy of 20 eV (a) and (c) and one for the low energy case where the outgoing electrons have an energy of 5 eV (b) and (d). In each case, the data show similar trends for both the molecule and atom. At the higher energy the cross section has a strong intensity in the forward direction which decreases rapidly with higher angles. The TDCS measured for neon only has a small increase for scattering angles beyond 110°, in contrast to CH_4, which shows a significant rise at angles greater than 110°. For the low energy case the triple peak structure noted in

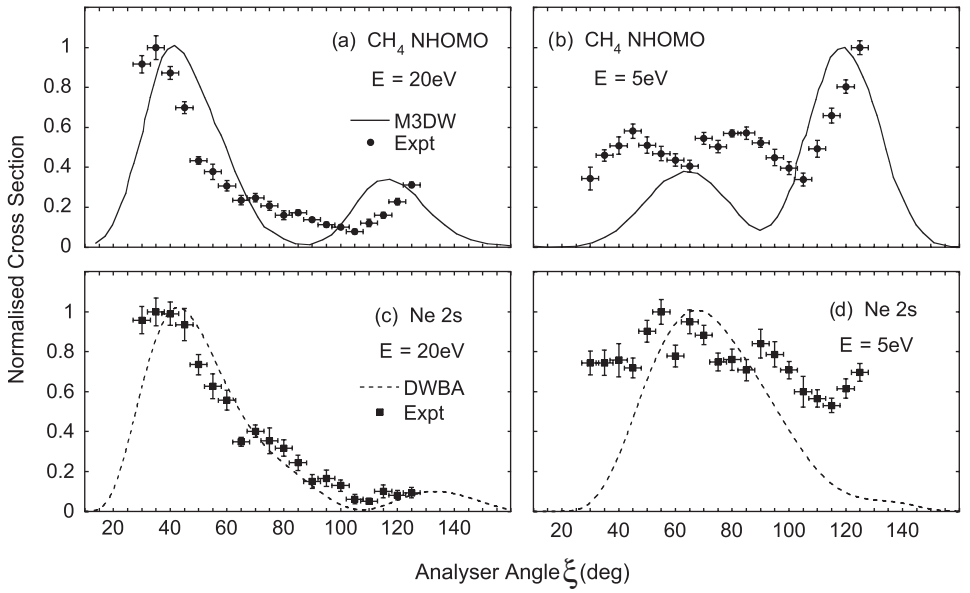

FIG. 7. TDCS for the equivalent states within the isoelectronic species, i.e., the $2a_1$ orbital of CH_4 and the 2s inner atomic state of Ne. The upper figures show results for the molecule at 20 and 5 eV outgoing energies, as in Fig. 4. The bottom panel shows the TDCS from the 2s state of neon collected under the same kinematics. The experimental data (points) are compared with theoretical predictions from the distorted wave calculations (solid line) for CH_4 and the distorted wave born approximation (dotted line) for neon.

Fig. 5 is seen in both targets, although for neon the scatter in the data makes this less clear than for CH_4. The maximum in the forward direction for neon occurs at higher angles than for CH_4. There is now a clear minimum around 115° for neon, whereas this minimum occurs at ~105° in CH_4. The cross section for CH_4 at higher angles is significantly larger than for forward scattering, in contrast to neon that does not show this effect at angles that are accessible within the spectrometer.

The qualitative similarities in the experimental cross sections for the two targets corroborate the premise that the target orbitals are similar. The comparison between the data and theory is quite good for neon at the higher energy [Fig. 7(c)]. By contrast, at low energies the theoretical TDCS does not emulate the data and is different for the two targets. With all nuclear charge placed at the centre of mass, theory only predicts a single peak for low energy while experiment appears to have a small three-lobe structure superimposed on a large single peak. The small three-lobe structure for Ne indicates that the strong three-lobes found for the $2a_1$ state on CH_4 arises from more than scattering from the H-nuclei. Since theory is not significantly better for the atomic target at low energies, this suggests that the spherical averaging process is not the sole source of discrepancy between experiment and theory, and that other approximations in the calculation must be playing a significant role at these energies, such as using distorted waves calculated on spherically symmetric molecular potentials that do not depend on the orientation of the molecule.

V. CONCLUSIONS

Experimental (e,2e) data for ionization of methane in the low energy regime using a coplanar symmetric geometry have been compared with a molecular three-body distorted wave approximation (M3DW). A comparison between the ϕ_{DY}^{OAMO} and experiment was made via high energy EMS results. Good agreement was found for both states. However, agreement between theory and experiment is somewhat mixed for low energies and rather surprisingly the best agreement was found for the outermost $1t_2$ molecular state, which has a change in parity through the molecular centre. By contrast, since the $2a_1$ molecular orbital is almost spherical in nature and does not have parity inversion, it was expected that inaccuracies introduced in the spherical averaging process would be minimized for this orbital, so that the theoretical result might be in better agreement with experiment. This was found not to be the case.

A comparison was made between the isoelectronic atomic and molecular cross sections. The theoretical atomic cross sections were in noticeably better agreement with experiment for higher energies but not low energies. This suggests that the molecular nature of the target is not the only cause of disagreement. It may be that the low energies used in these measurements are revealing limitations in the model due to the approximations that are used. Since the $2a_1$ state of CH_4 and the 2s state of neon are both inner states, it may also be that nuclear scattering plays a more predominant role that is not being properly treated. More experimental and theoretical work is clearly necessary to try to explain these differences.

ACKNOWLEDGMENTS

This work was supported by the University of Manchester and the US National Science Foundation under Grant. No. PHY-0757749. K.L.N. would like to thank the Royal Society for a Newton International Fellowship. We would also like to thank Sadek Mohammed Fituri Amami (Missouri University of Science and Technology) for providing the DWBA Ne 2s cross sections.

[1] J. Tennyson, Phys. Rep., Phys. Lett. **491**, 29 (2010).
[2] S. Bellm, J. Lower, R. P. McEachran, E. Weigold, C. Ryan-Andrewson and D. H. Madison, Phys. Rev. A **78**, 062707 (2008).
[3] D. V. Fursa, C. J. Bostock, and I. Bray, Phys. Rev. A **80**, 022717 (2009).
[4] J. Colgan, M. Foster, M. S. Pindzola, I. Bray, A. T. Stelbovics, and D. V. Fursa, J. Phys. B. **42**, 145002 (2009).
[5] C. J. Colyer, S. M. Bellm, B. Lohmann, G. F. Hanne, O. Al-Hagan, D. H. Madison, and C. G. Ning, J. Chem. Phys. **133**, 124302 (2010).
[6] C. J. Colyer, M. A. Stevenson, O. Al-Hagan, D. H. Madison, C. G. Ning, and B. Lohmann, J. Phys. B. **42**, 235207 (2009).
[7] A. Lahmam-Bennani, E. M. S. Casagrande, and A. Naja, J. Phys. B. **42**, 235205 (2009).
[8] D. S. Milne-Brownlie, S. J. Cavanagh, B. Lohmann, C. Champion, P. A. Hervieux, and J. Hanssen, Phys. Rev. A **69**, 032701 (2004).
[9] C. Champion, C. D. Cappello, S. Houamer, and A. Mansouri, Phys. Rev. A **73**, 012717 (2006).
[10] A. Lahmam-Bennani, A. Naja, E. M. S. Casagrande, N. Okumus, C. Dal Cappello, I. Charpentier, and S. Houamer, J. Phys. B. **42**, 165201 (2009).
[11] K. L. Nixon, A. J. Murray, O. Al-Hagan, D. H. Madison, and C. G. Ning, J. Phys. B. **43**, 035201 (2010).
[12] C. Kaiser, D. Spieker, J. F. Gao, M. Hussey, A. Murray, and D. H. Madison, J. Phys. B. **40**, 2563 (2007).
[13] M. J. Hussey and A. J. Murray, J. Phys. B. **38**, 2965 (2005).
[14] I. Toth and L. Nagy, J. Phys. B. **43**, 135204 (2010).
[15] D. H. Madison and O. Al-Hagan, J. Phys. B. **2010**, 367180.
[16] V. M. Sivakumar, A. R. Mohamed, A. Z. Abdullah, and S. P. Chai, J. Nanomater., **2010**, 395191 (2010).
[17] D. J. Fu, X. R. Zeng, J. Z. Zou, L. Li, X. H. Li, and F. Deng, J. Alloys Compd. **486**, 406 (2009).
[18] X. S. Li, C. W. Magnuson, A. Venugopal, J. H. An, J. W. Suk, B. Y. Han, M. Borysiak, W. W. Cai, A. Velamakanni, Y. W. Zhu, L. F. Fu, E. M. Vogel, E. Voelkl, L. Colombo, and R. S. Ruoff, Nano Lett. **10**, 4328 (2010).
[19] Z. P. Chen, W. C. Ren, B. L. Liu, L. B. Gao, S. F. Pei, Z. S. Wu, J. P. Zhao, and H. M. Cheng, Carbon **48**, 3543 (2010).
[20] F. Wang, J. Mol. Struct.Theochem **678**, 105 (2004).
[21] S. A. C. Clark, T. J. Reddish, C. E. Brion, E. R. Davidson, and R. F. Frey, Chem. Phys. **143**, 1 (1990).
[22] S. T. Hodd, E. Weigold, I. E. McCarthy, and P. J. O. Teubner, Nature (London) Phys. Sci. **245**, 65 (1973).
[23] E. Weigold, S. Dey, A. J. Dixon, I. E. McCarthy, and P. J. O. Teubner, Chem. Phys. Lett. **41**, (1976).
[24] R. Cambi, G. Ciukko, A. Sgamellotti, F. Tarantelli, R. Fantoni, A. Giardini-Guidoni, and A. Sergio, Chem. Phys. Lett. **41**, 295 (1981).
[25] A. J. Murray, B. C. H. Turton, and F. H. Read, Rev. Sci. Instrum. **63**, 3346 (1992).
[26] A. J. Murray and F. H. Read, Phys. Rev. A **47**, 3724 (1993).
[27] A. J. Murray and D. Cvejanovic, J. Phys. B. **36** (2003).
[28] J. F. Gao, J. L. Peacher, and D. H. Madison, J. Chem. Phys. **123**, 204302 (2005).
[29] J. F. Gao, D. H. Madison, and J. L. Peacher, J. Chem. Phys. **123**, 204314 (2005).
[30] J. F. Gao, D. H. Madison, and J. L. Peacher, J. Phys. B. **39**, 1275 (2006).

[31]C. T. Lee, W. T. Yang, and R. G. Parr, Phys. Rev. B **37**, 785 (1988).
[32]C. F. Guerra, J. G. Snijders, G. te Velde, and E. J. Baerends, Theor. Chem. Acc. **99**, 391 (1998).
[33]S. J. Ward and J. H. Macek, Phys. Rev. A **49**, 1049 (1994).
[34]J. B. Furness and I. E. McCarthy, J. Phys. B. **6**, 2280 (1973).
[35]J. P. Perdew and A. Zunger, Phys. Rev. B **23**, 5048 (1981).
[36]N. T. Padial and D. W. Norcross, Phys. Rev. A **29**, 1742 (1984).
[37]E. Weigold and I. E. McCarthy, *Electron Momentum Spectroscopy* (Kluwer/Plenum, New York, 1999).